Research Article Vol. 13, No. 6 / 1 Jun 2022 / Biomedical Optics Express 3161
Biomedical Optics EXPRESS

Bessel-beam illumination Raman microscopy

KAZUKI BANDO,[1] SHUMPEI YABUUCHI,[1] MENGLU LI,[1,2] TOSHIKI KUBO,[1] RYOSUKE OKETANI,[1] NICHOLAS I. SMITH,[3] AND KATSUMASA FUJITA[1,2,4,*]

[1]*Department of Applied Physics, Osaka University, 2-1 Yamadaoka, Suita, Osaka 565-0871, Japan*
[2]*AIST-Osaka University Advanced Photonics and Biosensing Open Innovation Laboratory, National Institute of Advanced Industrial Science and Technology (AIST), 2-1 Yamadaoka, Suita, Osaka 565-0871, Japan*
[3]*Immunology Frontier Research Center, Osaka University, 2-1 Yamadaoka, Suita, Osaka 565-0871, Japan*
[4]*Institute for Open and Transdisciplinary Research Initiatives, Osaka University, 2-1 Yamadaoka, Suita, Osaka 565-0871, Japan*
[*]*fujita@ap.eng.osaka-u.ac.jp*

Abstract: We demonstrate the use of Bessel beams for side illumination slit-scanning Raman imaging for label-free and hyperspectral analysis of cell spheroids. The background elimination by the side illumination and the aberration-resistant Bessel beam drastically improves the image contrast in Raman observation, allowing label-free investigation of intracellular molecules in thick biological samples. Live cell spheroids were observed to confirm the improvement in image contrast and background reduction with Bessel illumination compared to conventional epi-line illumination.

1. Introduction

Raman microscopy has attracted much attention as a new tool in biology and medicine due to its capability to provide label-free imaging of biological samples and their conditions [1,2]. In recent years, the development of high-speed Raman imaging techniques using both spontaneous and coherent Raman scatting have begun to bridge the gap between being limited to cells to thicker tissue samples [3–6]. In particular, cell spheroids and organoids are attracting attention because of functionality closer to actual tissues, compared to 2D cell cultures [7–9], and label-free evaluation is necessary for their application in pharmaceutical and medical uses, especially for drug development and regenerative medicine [10,11].

Raman imaging for label-free analysis of 3D cultured cells have been demonstrated [12–15], achieving spectral and spatial resolution sufficient to support the use as a tool to determine cell differentiation, material-cell interactions, and dynamic changes in cellular composition. However, observing the deeper parts of biological samples with rich biochemical information is still highly challenging. Spontaneous Raman microscopy, which provides detailed biochemical information and is well-suited for characterizing the phenotypes and behavior of individual cells in complex environments, is strongly constrained by weak signals and scattering from out of focus planes. These make it difficult to observe thick samples like spheroids by Raman imaging. Label-free evaluation of such samples has been highly anticipated to have various applications in the pharmaceutical and medical fields. The label-free assessment is also particularly beneficial for these samples because fluorescence staining of 3D cell samples often fails due to the unsuccessful penetration of fluorescent probes into the tissue.

In this paper, we propose the use of Bessel-beam illumination in slit scanning Raman microscopy to enable label-free observation and analysis of cell spheroids, where a Bessel beam illuminates a sample from the side to produce Raman scattering at the positions conjugated to the entrance slit of the spectrophotometer for hyperspectral Raman detection. With this configuration,

#456138 https://doi.org/10.1364/BOE.456138
Journal © 2022 Received 14 Feb 2022; revised 20 Apr 2022; accepted 20 Apr 2022; published 3 May 2022

Biomedical Optics EXPRESS

the background signal from the out of focus planes, surrounding medium, and optical components can be efficiently eliminated and allow observation of thick samples. In addition, due to the self-repairing effect of the Bessel beam [16], it is beneficial to reduce coherent artifacts on the line illumination induced during the light propagation through the sample. The benefit of side illumination has also been shown using light-sheet illumination in Raman microscopy in previous wide-field imaging studies [17–19], where the coherent artifacts significantly affect the image quality also. Our study shows that the combination of the Bessel illumination and the slit-confocal detection can drastically improve the capability of hyperspectral Raman imaging and analysis of tissues samples. We develop Bessel-beam illumination Raman microscopy and confirm the advantages in the imaging properties over conventional epi-line illumination Raman microscopy with cell spheroid samples.

2. Result

2.1. Construction and PSF calculation of Raman microscopy using Bessel and epi-line illumination

We constructed an optical system of a Raman microscope that employs side illumination using a Bessel beam as shown in Fig. 1. We used a 532 nm wavelength laser and an axicon prism to produce a Bessel beam that was introduced from the side of the sample through a water-immersion objective lens with an NA of 0.6. Raman scattering produced along the Bessel beam in the sample was imaged on the entrance slit of a spectrophotometer via an NA-0.8 water-immersion objective lens to obtain a hyper-spectral line image by a cooled CCD camera, enabling high-speed Raman imaging with parallel detection of 400 Raman spectra along the y-axis. The combination and selection of objective lenses were constrained in part by whether it was physically possible to place them in the setup and by the size of the observed sample that could be placed. Representative combinations of objective lenses that can be used for Bessel-illumination Raman microscopy are shown in Table S1. We also implemented an optical path to induce Raman scattering by epi-line illumination using a line-shaped focus to be able to compare the imaging properties between the Bessel and conventional epi-line illumination modes. Two imaging modes can be switched by using the flipper mirror in Fig. 1(a). We set the polarization of the Bessel illumination to the x-direction so that the detection objective lens can efficiently collect the induced Raman scattering. The slit width of the spectrophotometer was set to 1 Airy unit so that the spatial resolution for the z-direction can also be realized by the slit confocal effect [20]. The detail of the optical setup is shown in Fig. S1.

We evaluated the effective point-spread function (PSF) of the developed microscopes, which were calculated as the product of illumination PSF and detection PSF of the optics. As shown in Fig. 1(b)-(e), the Bessel beam illumination effectively reduces the elongation of the PSF for the z-direction compared to that in the epi-line illumination, indicating that the Bessel illumination can improve the axial resolution and the background elimination. In Bessel beam imaging, the side lobes can be problematic, however in our illumination mode, the entrance slit reduces the effect of side lobes on the image formation and is therefore a key factor in the realization of isotropic spatial resolution for all directions. As a drawback, we can also confirm that the lower NA of the illumination objective lens for the Bessel illumination resulted in the lower spatial resolution for the x-direction.

2.2. Comparison between Bessel and epi-line illumination

To compare the imaging property in observation of biological specimens, we observed fixed HeLa cell spheroids on quartz substrates. Raman images were obtained by scanning the Bessel and epi-line illumination for the y-direction at the same position of the sample. The intensity distributions of Raman peaks on y-z plane were plotted in Fig. 2(a)-(h). From the comparisons

Biomedical Optics EXPRESS

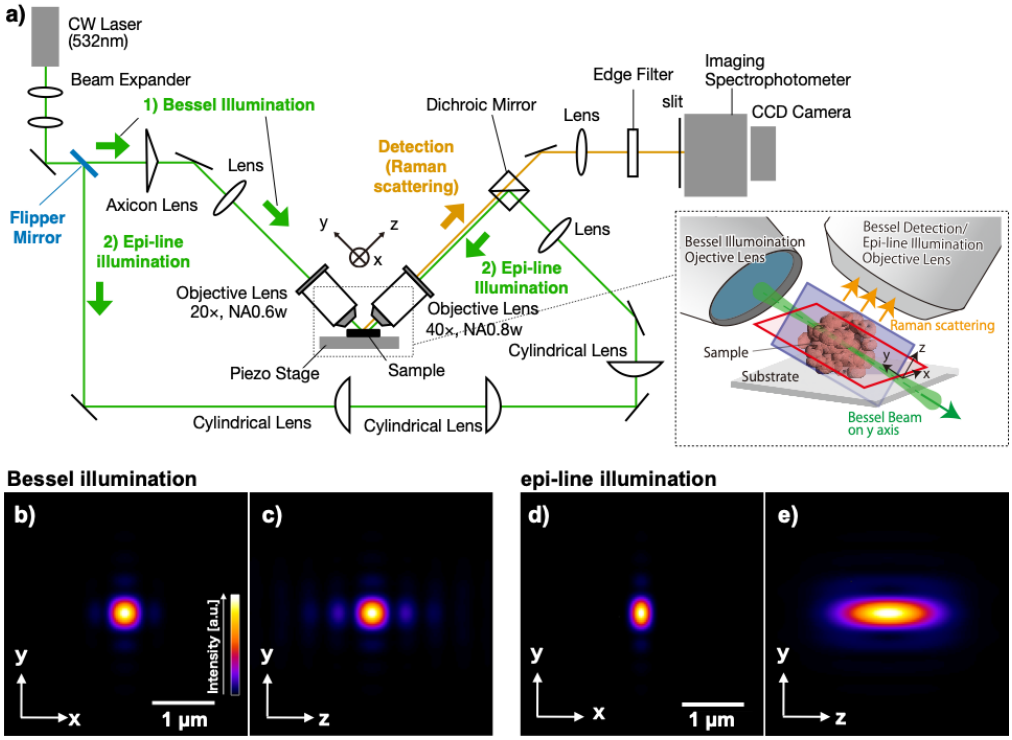

Fig. 1. Raman microscopy using the Bessel- and epi-line illumination. a) An optical setup of Raman microscope using the Bessel and epi-line illumination. The two illumination modes can be switched by using the flipping mirror, allowing comparison of imaging properties in the illumination modes. The inset is a 3D schematic view of the dotted square area around the sample. This is the excitation light in the case of Bessel illumination. b-e) The calculated effective point-spread-functions on *x*-*y* and *y*-*z* planes in the Bessel and the epi-line illumination modes.

between Fig. 2(a)-(d) and (e)-(h), we can confirm that the Bessel illumination mode visualized the interior of the spheroid more clearly than that by the epi-illumination mode. The light diffraction affected the epi-line illumination mode and caused non-uniform illumination in the *y*-direction. On the other hand, in the Bessel illumination mode, the self-repairing nature of the Bessel beam [16] effectively reduced the diffraction effect. It maintained the uniform intensity distribution on the illumination line, which was also confirmed by imaging a polystyrene bead in agarose gel, as shown in Fig. 3. The self-repairing effect of the Bessel beam effectively reduces the sample-induced aberration in the Bessel illumination mode. On the other hand, in epi-line mode, the diffraction at the border between agarose and polystyrene produced a shadow effect resulting in non-uniform illumination and poor imaging quality. To exclude shadow effects and to compare background light, line profiles were taken and compared vertically in Fig. 3(c). Intensity profiles showed that Bessel illumination led to a 1.66-fold suppression of background light compared to epi-line illumination in this measurement.

We also found that the side illumination effectively reduces the contribution of the quartz substrate to the cell contrast. The comparison of Raman spectra obtained at the same position in Fig. 2(d) and 2(h) confirms that the background signal from the out-of-focus planes, especially from the substrate, is effectively reduced, as indicated by the black arrows in Fig. 2(i). The elimination of the broad spectra from non-cellular components can improve the detection

Biomedical Optics EXPRESS

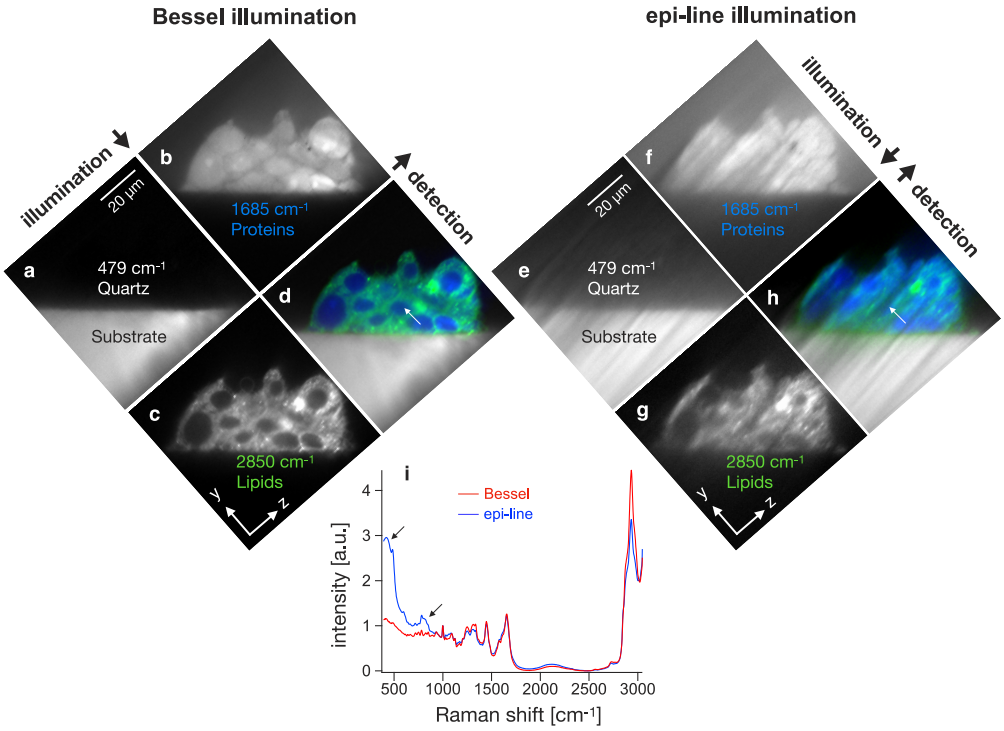

Fig. 2. Raman images of a fixed HeLa cell spheroid. Raman images by using Bessel (a-d) and epi-line (e-h) illumination. The Raman images were reconstructed by plotting the peak intensities at 479 cm^{-1} (a, e), 1685 cm^{-1} (b, f), and 2850 cm^{-1} (c, g), which can be assigned to quartz (substrate), proteins, and lipids, respectively. The color-merged Raman images are shown in d and h. Scale bars, 20 μm. i) The Raman spectra measured at the nucleus region indicated in the arrows in d and h. The intensities of the spectra were normalized by the phenylalanine peak at 1000 cm^{-1}.

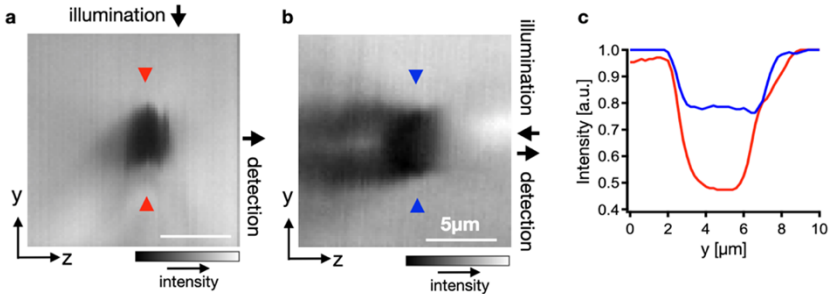

Fig. 3. Raman images of agarose containing a polystyrene bead and water obtained by a) Bessel and b) epi-line illumination microscopy. The images were constructed by the Raman intensity of water (averaged signal between 3200 cm^{-1} and 3700 cm^{-1}). Scale bars: 5 μm. c) The intensity profiles between the arrow beads in a) (red) and b) (blue) show the background reduction effect in the Bessel illumination mode.

Biomedical Optics EXPRESS

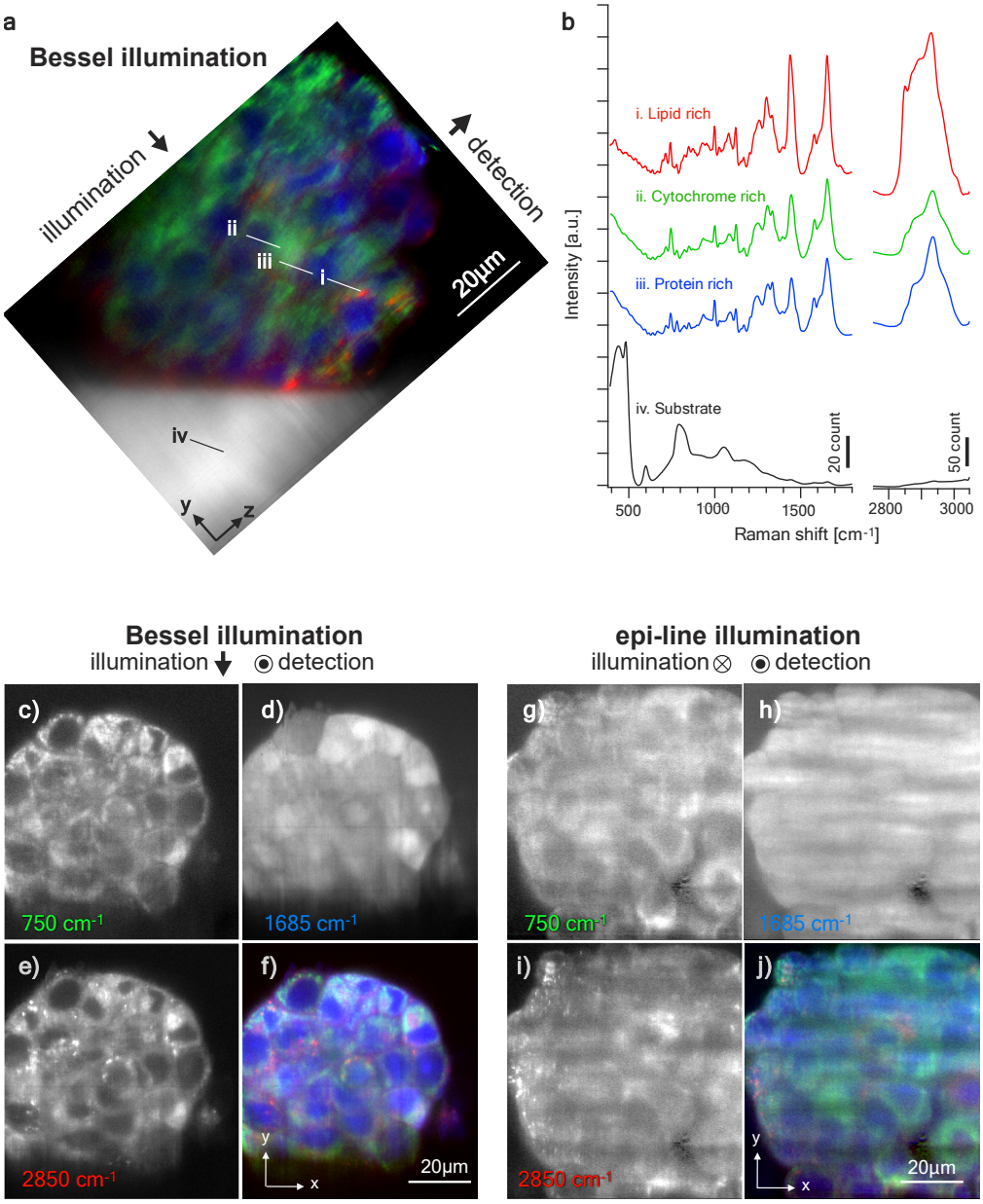

Fig. 4. Raman images of living HeLa cell spheroids. a) *y*-*z* cross-section Raman image of a living cell spheroid with a diameter of around 80 μm observed by Bessel-illumination Raman microscopy, reconstructed color-merged Raman image using the Raman peak intensities at 479 cm^{-1} as white, 750 cm^{-1} as green, 1685 cm^{-1} as blue, and 2850 cm^{-1} as red, which can be assigned to quartz (substrate), cytochromes, protein, and lipids, respectively. b) Typical Raman spectra from the point indicated with i-iv in a. The plots of Raman spectra were vertically shifted for clear visibility. *x*-*y* cross-section Raman images of a living cell spheroid with a diameter of around 60 μm observed by Bessel (c-f) and epi-illumination (g-j) Raman microscopy, reconstructed using the Raman peak intensities at 750 cm^{-1} (c, g), 1685 cm^{-1} (d, h), and 2850 cm^{-1} (e, i), which can be assigned to cytochromes, proteins, and lipids, respectively. f and j are color-merged Raman images using c-e and g-i, respectively. Scale bars, 20 μm.

Biomedical Optics EXPRESS

sensitivity and the analytical capability of Raman microscopy. Together, these comparisons confirm that Bessel beam illumination can be used to achieve hyperspectral Raman imaging of a thick specimen.

2.3. Imaging of HeLa cell spheroids in living conditions

We examined the ability of Bessel illumination Raman microscopy to image large cell spheroids in living conditions, as shown in Fig. 4(a). The cell distribution at the bottom of the spheroid can also be recognized through the 80 μm tissue layer, although the image contrast is somewhat degraded due to the sample-induced aberration at the detection. Figure 4(b) shows the Raman spectra obtained in the points indicated by i-iv) in Fig. 4(a), which show that the Raman peaks that can be used to characterize the molecular components in the spheroid can still be measured, with identification of each individual cell location. We also compared the Raman images of *x*-*y* cross-section obtained from the middle part of a live cell spheroid with a diameter of around 60 μm by using the Bessel and epi-illumination Raman microscopes, as shown in Fig. 4(c)-(f) and 4(g)-(j), respectively. The non-uniform illumination for the *y*-direction was confirmed in the *x*-*y* cross-section image by the epi-line illumination, but not by the Bessel illumination, where the self-repairing effect of the Bessel beam was also beneficial in *x*-*y* cross-section imaging. Thanks to the self-repairing effect, the difference of protein concentration between the surface and the interior of the spheroid is clearly recognized in the Bessel illumination mode, but not in the epi-line illumination mode. In addition, the localization of lipid droplets within the spheroids is observed by Bessel illumination. These results confirm the advantages of Bessel beam illumination in Raman microscopy to investigate cell properties in deep regions of cell spheroids without labeling.

3. Discussion and conclusions

In this paper, we proposed the use of Bessel-beam illumination in slit-scanning Raman microscopy for observation of thick biological samples and demonstrated the improvements in the image contrast and practical resolutions in the observations of spheroids compared to conventional epi-line illumination Raman microscopy. The background reduction and isotropic spatial resolution achieved by the combination of the Bessel illumination and the slit-confocal detection drastically improved the imaging property of Raman microscopy in the observation of thick cell samples.

Aside from expanding the range of samples observable by Raman microscopy, this technique has additional advantages when considering that Raman scattering is an inefficient physical interaction and typically requires a relatively high amount of excitation light. Especially in living biological specimens, where non-invasiveness is critical, it is important to devise ways to reduce photodamage. Our experiment found that the Bessel illumination requires less illumination power to obtain the same amount of Raman signal under epi-illumination. This is advantageous to reduce photodamage in 3D live-cell imaging, in some ways, similar to what has been achieved in light-sheet fluorescence microscopy [21,22]. In the field of regenerative medicine and drug discovery using 3D samples like spheroids, there is a demand for repeated observations over time, and one of the important requirements is to observe the cells while they are alive with minimal optical damage.

Although we were able to visualize the cell distributions in the spheroids, we also confirmed the degradation of the spatial resolution and the contrast of the cell images at the bottom of the spheroid, which is presumably due to the aberrations induced by the ununiform distribution of the refractive index in the detection path. Such aberrations can be reduced by introducing adaptive optics [23,24] in the detection path. We expect that this will allow for more detailed elucidation of the internal information.

In our measurement, we used the 532 nm illumination light that shows the resonance Raman scattering from the molecules, such as cytochromes and flavin, as demonstrated in the literature

Biomedical Optics EXPRESS

[25–27]. Therefore, the Raman signal of those molecules can be enhanced by the resonance effect and specifically detected by Raman imaging. For the observation of thick samples, using a longer wavelength should be useful. The use of longer wavelengths, such as near-infrared light, can also reduce the damage to samples and allow long-term observation of living samples. However, near-infrared light exhibits smaller Raman scattering cross-sections than visible light and has less chance of receiving the benefits of the resonant Raman scattering for signal enhancement. It is important to select the excitation wavelength by considering the trade-off between the depth penetration and the signal amount depending on the target.

It would also be possible to use a Gaussian beam for the side and wide-area illumination [28,29]. Compared with the Gaussian beam, the Bessel beam exhibits strong side-lobes, which may degrade the axial resolution when it is used for side illumination [21]. However, in combination with the slit-scanning Raman microscopy, the confocal effect of the slit detection can reduce the effect of the side lobes on the effective PSF, as shown in Fig. 1(c). Aside from the side lobes, the Bessel beam shows the advantages in the length and the uniformity of the light distribution along the beam propagation direction compared to the Gaussian beam, as shown in Fig. S1. Therefore, the slit confocal detection can successfully introduce the above benefits of the Gaussian beams into side-illumination microscopy.

Raman observation of cell spheroids or organoids derived from iPS and ES cells is a critical application in pharmaceutical research and regenerative medicine because the label-free evaluation of those samples is in high demand for non-destructive observation of spheroids and organoids [12,13]. As demonstrated using 2D cultured cells, Raman spectroscopy is advantageous to investigate the cell conditions and differentiation status without labeling. The hyperspectral Raman imaging of the spheroid interior will allow us to evaluate the differentiation and maturation of iPS and ES cells in the spheroid. The lack of methods for non-destructive evaluation of different cell populations within complex culture environments has hampered their application in pharmaceutical developments and medical treatments. More specifically, in terms of quality control, the ability to evaluate the cell states and spheroid development without labeling will reduce the time and cost for cell production and contribute to reliable and repeatable mass production of spheroids for the practical use.

Bessel illumination Raman microscopy can also be beneficial to improve the sensitivity in low concentration samples where the existence of background signal essentially limits the capability of weak signal detection. As shown in Fig. 2(i), the background signal from the out-of-focus planes is effectively reduced by the side illumination, allowing us to detect weak signals that may otherwise be hidden by shot noise if the background contribution is high. The improvement in the sensitivity due to this effect is significant enough to allow broadening of the applications in small molecule imaging, super-multiplex imaging, and metabolic imaging using Raman tags and probes, where targets have often been limited due to the low sensitivity [30–33]. As a more general principle, low background, Raman microscopy that can maintain sufficient spectral and spatial resolution in deeper samples can expand the versatility of Raman spectroscopy in numerous research and industrial fields, including material, biological, pharmaceutical, and medical fields.

4. Methods

4.1. Calculation of point-spread-functions

The effective PSFs of the systems are calculated by using the following formula.

$$h_{\mathrm{eff}}(x, y, z) = h_{\mathrm{ex}}\ (x, y_s, z)(\ h_{\mathrm{det}}(x, y, z) \otimes_{1\mathrm{D}} \mathrm{S}(x))$$

Here h_{ex}, h_{det}, and S are the excitation PSF, the detection PSF, and the transmission distribution of the confocal slit, respectively. x, y, and z are the position coordinates in object space as in Fig. 1

Biomedical Optics EXPRESS

and y_s is the position of an object in the y-direction. $\otimes_{1D}$ denotes the 1-D convolution integral for the direction perpendicular to the long axis of the slit (the x-direction), which was performed to take into account the confocal effect by the slit. The excitation PSF of the line illumination in the epi-line illumination system was calculated using scalar diffraction theory [34]. The NA of the objective lens was assumed 0.8 for line illumination. The excitation PSF of the Bessel illumination and h_{det} were calculated by using vector diffraction theory [35]. To calculate the excitation PSF of Bessel beam, it was assumed that an annular pupil with a size corresponding to an NA of 0.6 was irradiated. A linear polarization in the x-direction was assumed in the calculation, which was the same as the experimental condition. Also, a point object placed at $y = 0$ was assumed as a sample. In calculation of the detection PSF, an objective lens of NA 0.8 was assumed. The wavelength of excitation and detection were both assumed to be 532 nm. The width of the slit was set to 1 Airy unit (AU) for the wavelength of 532 nm.

4.2. Culturing HeLa cell spheroids

HeLa spheroids were formed using a commercially available 35-mm dish with a low-adhesive micro-patterned bottom (Iwaki, Ezsphere, 4000–900). When HeLa cells reached 70–80% confluency, they were harvested and seeded into the 35-mm dish at a density of 50 cells/spheroid in Dulbecco's modified Eagle medium (Wako, DMEM, 043-30085) supplemented with 10% fetal bovine serum (Biowest, S1400-500), 2 mM L-glutamine, 100 units/ml penicillin and 100 µg/ml streptomycin (Gibco, 10378-016). HeLa cells were incubated at 37 °C in an atmosphere of 5% CO_2 for 2∼3 days to form spheroids. The spheroids were collected and plated on an 18 mm quart substrates precoated with 0.01% type I collagen solution (Functional Peptide Institute, IFP9660) to promote adhesion. The spheroids were allowed to adhere to the quartz substrates for 1 hour. They were then washed twice with warm PBS and immersed in a Hank's Balanced Salt Solution without phenol red (Wako, 082-08961). For experiments using fixation, which was done to compare Bessel and epi-illumination Raman setups (Fig. 2), after the spheroids attached to quartz substrates, samples were washed twice by PBS and fixed in 4% paraformaldehyde for 20 min. After rinsing twice with PBS, the fixed spheroids were observed by Raman microscope.

4.3. Raman imaging

The illumination power at the sample was 75 mW and 125 mW for the Bessel and epi-line illumination modes, respectively (Fig. 3, 4). The exposure time at each position was 3 seconds for both modes. The sample was scanned in z- or x- directions to obtain either y-z or x-y cross-section images.

4.4. Raman spectrum processing and image reconstruction

After Raman observation, hyperspectral Raman data cubes were processed using a previously developed method [4]. Cosmic rays were removed by a median filter, and then noise reduction was performed by singular value decomposition. Loading vectors contributing to cell contrast were selected to reconstruct Raman images. The Raman images of the targeted Raman shifts were reconstructed by subtracting the Raman intensity of the peaks and valleys. The broad fluorescence background was removed for Fig. 4(b) by polynomial fitting [36].

Funding. JST-Mirai Program (JPMJMI20G3); JST-CREST program (PMJCR1925).

Acknowledgments. The authors thank Ryosuke Morisaki, Tomoyuki Murashima, and Takuma Shibata for advice on sensitivity evaluation and optical setup construction. This work was partially supported by JST-Mirai Program and JST-CREST program under Grant Numbers JPMJMI20G3 and JPMJCR1925, Japan.

Disclosures. KB and KF are the inventors of a patent on Bessel-illumination Raman microscopy submitted by Osaka University.

Data availability. All data used in this paper are available upon reasonable request.

Biomedical Optics EXPRESS

Supplemental document. See Supplement 1 for supporting content.

References

1. H. J. Butler, L. Ashton, B. Bird, G. Cinque, K. Curtis, J. Dorney, K. Esmonde-White, N. J. Fullwood, B. Gardner, P. L. Martin-Hirsch, M. J. Walsh, M. R. McAinsh, N. Stone, and F. L. Martin, "Using Raman spectroscopy to characterize biological materials," Nat. Protoc. **11**(4), 664–687 (2016).
2. C. Krafft, M. Schmitt, I. W. Schie, D. Cialla-May, C. Matthäus, T. Bocklitz, and J. Popp, "Label-free molecular imaging of biological cells and tissues by linear and nonlinear Raman spectroscopic approaches," Angew. Chem. Int. Ed. **56**(16), 4392–4430 (2017).
3. K. Hamada, K. Fujita, N. I. Smith, M. Kobayasi, Y. Inouye, and S. Kawata, "Raman microscopy for dynamics molecular imaging of living cells," J. Biomed Opt. **13**(4), 044027 (2008).
4. A. F. Palonpon, J. Ando, H. Yamakoshi, K. Dodo, M. Sodeoka, S. Kawata, and K. Fujita, "Raman and SERS microscopy for molecular imaging of live cells," Nat. Protoc. **8**(4), 677–692 (2013).
5. C. W. Freudiger, W. Min, B. G. Saar, S. Lu, G. R. Holtom, C. He, J. C. Tasai, J. X. Kang, and X. S. Xie, "Label-free biomedical imaging with high sensitivity by stimulated Raman scattering microscopy," Science **322**(5909), 1857–1861 (2008).
6. A. Zumbusch, G. R. Holtom, and X. S. Xie, "Three-dimensional vibrational Imaging by coherent anti-Stokes Raman scattering," Phys. Rev. Lett. **82**(20), 4142–4145 (1999).
7. F. Pampaloni, E. G. Reynaud, and E. H. K. Stelzer, "The third dimension bridges the gap between cell culture and live tissue," Nat. Rev. Mol. Cell Biol. **8**(10), 839–845 (2007).
8. E. Fennema, N. Rivron, J. Rouwkema, C. van Blitterswijk, and J. de Boer, "Spheroid culture as a tool for creating 3D complex tissues," Trends Biotechnol. **31**(2), 108–115 (2013).
9. G. Rossi, A. Manfrin, and M. P. Lutolf, "Progress and potential in organoid research," Nat. Rev. Genet. **19**(11), 671–687 (2018).
10. K. Klein, A. M. Gigler, T. Aschenbrenner, R. Monetti, W. Bunk, F. Jamitzky, G. Morfill, R. W. Stark, and J. Schlegel, "Label-free live-cell imaging with confocal Raman microscopy," Biophys J. **102**(2), 360–368 (2012).
11. K. J. I. Ember, M. A. Hoeve, S. L. McAughtrie, M. S. Bergholt, B. J. Dwyer, M. M. Stevens, K. Faulds, S. J. Forbes, and C. J. Campbell, "Raman spectroscopy and regenerative medicine: a review," npj Regen. Med. **2**(1), 12 (2017).
12. F. C. Pascut, S. Kalra, V. George, N. Welch, C. Denning, and I. Notingher, "Non-invasive label-free monitoring the cardiac differentiation of human embryonic stem cells *in-vitro* by Raman spectroscopy," Biochim. Biophys. Acta. **1830**(6), 3517–3524 (2013).
13. G. Pettinato, M. F. Coughlan, X. Zhang, L. Chen, U. Khan, M. Glyavina, C. J. Sheil, P. K. Upputuri, Y. N. Zakharov, E. Vitkin, A. B. D'Assoro, R. A. Fisher, I. Itzkan, L. Zhang, L. Qiu, and L. T. Perelman, "Spectroscopic label-free microscopy of changes in live cell chromatin and biochemical composition in transplantable organoids," Sci. Adv. **7**(34), eabj2800 (2021).
14. N. Jung, T. Moreth, E. H. K. Stelzer, F. Pampaloni, and M. Windbergs, "Non-invasive analysis of pancreas organoids in synthetic hydrogels defines material-cell interactions and luminal composition," Biomater. Sci. **9**(16), 5415–5426 (2021).
15. H. Kim, Y. Han, I. R. Suhito, Y. Choi, M. Kwon, H. Son, H. R. Kim, and T. H. Kim, "Raman spectroscopy-based 3D analysis of odontogenic differentiation of human dental pulp stem cell spheroids," Anal. Chem. **93**(29), 9995–10004 (2021).
16. V. Garcés-Chávez, D. McGloin, H. Melville, W. Sibbett, and K. Dholakia, "Simultaneous micromanipulation in multiple planes using a self-reconstructing light beam," Nature **419**(6903), 145–147 (2002).
17. I. Barman, K. M. Tan, and G. P. Singh, "Optical sectioning using single-plane-illumination Raman imaging," J. Raman Spectrosc. **41**(10), 1099–1101 (2010).
18. Y. Oshima, H. Sato, H. K. Kobayashi, T. Kimura, K. Naruse, and S. Nonaka, "Light sheet-excited spontaneous Raman imaging of a living fish by optical sectioning in a wide field Raman microscope," Opt. Express **20**(15), 16195–16204 (2012).
19. W. Müller, M. Kielhorn, M. Schmitt, J. Popp, and R. Heintzmann, "Ligh-sheet Raman micro-spectroscopy," Optica **3**(4), 452–457 (2016).
20. S. Kawata, R. Arimoto, and O. Nakamura, "Three-dimensional optical-transfer-function analysis for a laser-scan fluorescence microscope with an extended detector," J. Opt. Soc. Am. A **8**(1), 171–175 (1991).
21. T. A. Planchon, L. Gao, D. E. Milkie, M. W. Davidson, J. A. Galbraith, C. G. Galbraith, and E. Betzig, "Rapid three-dimensional isotropic imaging of living cells using Bessel beam plane illumination," Nat. Methods **8**(5), 417–423 (2011).
22. J. Huisken, J. Swoger, F. D. Bene, J. Wittbrodt, and E. H. Stelzer, "Optical sectioning deep inside live embryos by selective plane illumination microscopy," Science **305**(5686), 1007–1009 (2004).
23. C. Bourgenot, C. D. Saunter, J. M. Taylor, J. M. Girkin, and G. D. Love, "3D adaptive optics in a light sheet microscope," Opt. Express **20**(12), 13252–13261 (2012).
24. M. J. Booth, "Adaptive optical microscopy: the ongoing quest for a perfect image," Light Sci. Appl. **3**(4), e165 (2014).
25. M. Okada, N. I. Smith, A. F. Palonpon, H. Endo, S. Kawata, M. Sodeoka, and K. Fujita, "Label-free Raman observation of cytochrome c dynamics during apoptosis," Proc. Natl. Acad. Sci. USA **109**(1), 28–32 (2012).

Biomedical Optics EXPRESS

26. M. Ogawa, Y. Harada, T. Yamaoka, K. Fujita, H. Yaku, and T. Takamatsu, "Label-free biochemical imaging of heart tissue with high-speed spontaneous Raman microscopy," Biochem. Biophys. Res. Communn. **382**(2), 370–374 (2009).
27. E. Bendau, J. Smith, L. Zhang, E. Ackerstaff, N. Kruchevsky, B. Wu, J. A. Koutcher, R. Alfano, and L. Shi, "Distinguishing metastatic triple-negative breast cancer from nonmetastatic breast cancer using second harmonic generation imaging and resonance Raman spectroscopy," J. Biophotonics **13**(7), e202000005 (2020).
28. P. J. Keller, A. D. Schmidt, J. Wittbrodt, and E. H. Stelzer, "Reconstruction of zebrafish early embryonic development by scanned light sheet microscopy," Science **322**(5904), 1065–1069 (2008).
29. L. Shi, A. Rodríguez-Contreras, and R. R. Alfano, "Gaussian beam in two-photon fluorescence imaging of rat brain microvessel," J. Biomed. Opt. **19**(12), 126006 (2014).
30. H. Yamakoshi, K. Dodo, M. Okada, J. Ando, A. Palonpon, K. Fujita, S. Kawata, and M. Sodeoka, "Imaging of EdU, an alkyne-tagged cell proliferation probe, by Raman Microscopy," J. Am. Chem. Soc. **133**(16), 6102–6105 (2011).
31. L. Wei, Z. Chen, L. Shi, R. Long, A. V. Anzalone, L. Zhang, F. Hu, R. Yuste, V. W. Cornish, and W. Min, "Super-multiplex vibrational imaging," Nature **544**(7651), 465–470 (2017).
32. F. Hu, C. Zeng, R. Long, Y. Miao, L. Wei, Q. Xu, and W. Min, "Supermultiplexed optical imaging and barcoding with engineered polyynes," Nat. Methods **15**(3), 194–200 (2018).
33. L. Zhang, L. Shi, Y. Shen, Y. Miao, M. Wei, N. Qian, Y. Liu, and W. Min, "Spectral tracing of deuterium for imaging glucose metabolism," Nat Biomed. Eng. **3**(5), 402–413 (2019).
34. E. Dusch, T. Dorval, N. Vincent, M. Wachsmuth, and A. Genovesio, "Three-dimensional point spread function model for line-scanning confocal microscope with high-aperture objective," J. Microsc. **228**(2), 132–138 (2007).
35. B. Richards and E. Wolf, "Electromagnetic diffraction in optical systems, ii. structure of the image field in an aplanatic system," Proc. R. Soc. Lond. A **253**(1274), 358–379 (1959).
36. C. A. Lieber and A. M. Jansen, "Automated method for subtraction of fluorescence from biological Raman spectra," Appl. Spectrosc. **57**(11), 1363–1367 (2003).